CHIN. PHYS. LETT. Vol. 34, No. 11 (2017) 116101

Synthesis of Different TiO_2 Nanostructures and Their Physical Properties

T. Hoseinzadeh[1], Z. Ghorannevis[2], M. Ghoranneviss[1**], M. K. Salem[1], A. H. Sari[1]

[1]*Department of Physics, Science and Research Branch, Islamic Azad University, Tehran, Iran*
[2]*Department of Physics, Karaj Branch, Islamic Azad University, Karaj, Iran*

(Received 11 August 2017)

Titanium dioxide (TiO_2) nanosheet, nanorod and nanotubes are synthesized using chemical vapor deposition (CVD) and anodizing processes. TiO_2 nanosheets are grown on Ti foil which is coated with Au catalyst in CVD, TiO_2 nanorods are synthesized on treated Ti foil with HCl by CVD, and TiO_2 nanotubes are prepared by the three-step anodization method. Scanning electron microscopy shows the final TiO_2 structures prepared using three processes with three different morphologies of nanosheet, nanorod and nanotube. X-ray diffraction verifies the presence of TiO_2. TiO_2 sheets and rods are crystalized in rutile phase, and TiO_2 tubes after annealing turn into the anatase crystal phase. The optical investigations carried out by diffuse reflection spectroscopy reveal that the morphology of TiO_2 nanostructures influencing their optical response and band gap energy of TiO_2 is changed for different TiO_2 nanostructures.

PACS: 61.05.−a, 61.46.Np, 61.46.Km DOI: 10.1088/0256-307X/34/11/116101

Titanium dioxide is one of the most multifunctional semiconductors, used in a wide range of research activity. Various physical and chemical properties such as wide band gap, high chemical stability and low cost, make it applicable in photocatalysis, photovoltaics, sensors, lab-on-a-chip devices and blood-compatible implants.[1−7] In most of the applications, the morphology of TiO_2 is known to play an important role in performance of devices. For instance, in the case of dye and quantum dot solar cells, structures of the TiO_2 strongly affect the cell performance. Different morphology parameters such as roughness factor, grain boundaries, electron lifetime and crystallinity were found to be essential parameters in solar cell efficiencies.[8−13] Moreover, mesoporous structures based on TiO_2 nanoparticles were observed to be suitable for dye solar cells. On the other hand, the surface area of the mesoporous TiO_2 is not important in heterojunction quantum dot solar cells and it was found that one-dimensional structures show better electron transport and higher efficiencies in the case of these cells.[14] Therefore, in the present study, three different TiO_2 nanostructures of nanotubes, nanorods and nanosheets are synthesized under optimum conditions by different methods. We examine morphological aspects of the TiO_2 nanostructures on the basis of x-ray diffraction (XRD), scanning electron microscopy (SEM) and diffuse reflection spectra (DRS) experimental data.

Chemical vapor deposition (CVD) process is used to synthesize TiO_2 nanosheets. For removing the surface contamination, the Ti foils (0.25 thickness, 99.9% pure, Sigma Aldrich) were ultrasonically cleaned with ethanol, acetone and deionized water for 20 min, respectively, and then a thin film of Au is sputtered on the Ti foil surface. A horizontal tube furnace is used to oxidize the Ti foils and then the Ar gas is introduced into the furnace tube at a flow rate of 200 sccm for 4 h. Three different flows of gasses are used to study their effects on the morphologies of synthesized films. For the first sample, the furnace was heated to 850℃ with the rate of 30℃·min^{-1} and then oxygen gas at a constant flow rate of 100 sccm was introduced into the tube. The furnace temperature was held for 1.5 h at 850℃ and then naturally cooled to room temperature under Ar stream. For the second sample, after the system is purged with a pure Ar stream for 4 h, when the furnace is heated up to 850℃, ethanol was carried into the furnace tube by an Ar stream passing through a bottle containing ethanol, and the temperature was again held for 1.5 h. Finally the system under the Ar stream was cooled down to the room temperature. For the third sample, the system was purged and heated the same as the second sample, but the Ar stream passed through a bottle of acetone instead of ethanol. According to the SEM images shown in Fig. 1, comparing samples with three different annealing processes, different structures are obtained. The oxidation has a remarkable effect on the morphology of TiO_2 nanostructures. The use of the mixture of Ar with low concentration oxygen yielded a microcrystalline TiO_2 film, whereas the use of ethanol carried by Ar gave a randomly oriented nanowall and the use of acetone carried by Ar produced dense well-aligned nanosheet arrays.

CVD process is used to synthesize TiO_2 nanorods. For removing the surface contamination, the Ti foils (0.25 thickness, 99.9% pure, Sigma Aldrich) were ultrasonically cleaned with ethanol, acetone and deionized water for 20 min, respectively. Later the samples are etched in 30 wt% HCl at 80℃ for 10 min to remove the oxide layer on the surface, then these are washed with distilled water and finally dried in a vacuum oven at 40℃. A horizontal tube furnace was used to oxidize Ti foils and then the Ar gas was introduced into the furnace tube at a flow rate of 200 sccm for 4 h.

**Corresponding author. Email: ghoranneviss@gmail.com

To investigate the effects of these gasses during the films' synthesis on their morphologies, three different gasses were used. For the first sample, the furnace was heated up to the 850℃ with rate of 30℃·min^{-1} and then oxygen at a constant flow rate of 100 sccm was introduced into the tube. The furnace temperature was held for 1.5 h at 850℃ and then naturally cooled to room temperature under the Ar stream. For the second sample, after the system was purged with the Ar stream for 4 h, when the furnace was heated up to 850℃, ethanol was carried into the furnace tube by an Ar stream passing through a bottle containing ethanol, and the temperature was again held for 1.5 h. Finally the system was cooled to the room temperature under the Ar stream. For the third sample, the system was purged and heated the same as the previous sample, but the Ar stream passed through the bottle of acetone instead of ethanol. According to the SEM images shown in Fig. 2, the sample grown under Ar/acetone stream leads to the development of TiO_2 nanorods with more uniform features.

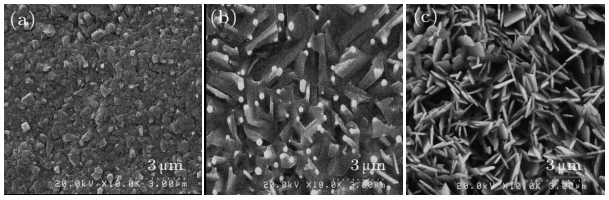

Fig. 1. SEM images of the nanosheets synthesized in CVD at 850℃ for 1.5 h: (a) under stream of Ar and O_2 flow, (b) under stream of Ar and C_2 H_6O (ethanol) flow, and (c) under stream of Ar and C_3 H_6O (acetone) flow.

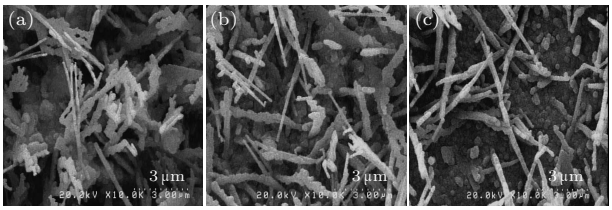

Fig. 2. SEM images of the nanorods synthesized in CVD at 850℃ for 1.5 h: (a) under Ar and O_2 flow, (b) under Ar and C_2 H_6O (ethanol) flow, and (c) under Ar and C_3 H_6O (acetone) flow.

In last part, three steps of anodization process were used to synthesize TiO_2 nanotubes. For removing the surface contamination, the Ti foils (0.25 thickness, 99.9% pure, Sigma Aldrich) were ultrasonically cleaned with ethanol, acetone and deionized water for 20 min in order and were dried by an N_2 stream. The electrolytic solution contained ethylene glycol ($C_2H_6O_2$), ammonium fluoride salt (NH_4F) and deionized water (DI). Electrochemical setup and the anodizing parameters such as concentration of electrolyte, process temperature and anodizing time were kept the same for all of the processes. Different voltages of 35, 45 and 55 V were applied to study the effect of the applied voltage on the TiO_2 grown samples. The Ti foil was anodized for 1 h in the first step. The hexagonal patterns on Ti foil surface were observed by ultra-sonication of the TiO_2 nanotube samples in methanol. The second step that the uniform TiO_2 nanotubes were grown was performed for 3 h in the same solution. The samples were ultra-sonicated in methanol again to remove the top of the tube, after the second anodization, and then dried by the N_2 stream. The TiO_2 nanotubes that were grown on the surface of the Ti foils are annealed in ambient air at 450℃ for 1 h with a heating ramp of 2.5℃·min^{-1}. After annealing, the third step of the anodization process was carried out for 1 h and finally dried by the N_2 stream. The effective approach, three-step anodization process, develops highly ordered crystallized and top open channel TiO_2 nanotubes. The optimum anodization voltage to grow top open and compacted arrays in electrolyte solution contained (2 v%) deionized water and (0.3 wt.%) NH_4F was about 55 V, reported in our previous work.[15]

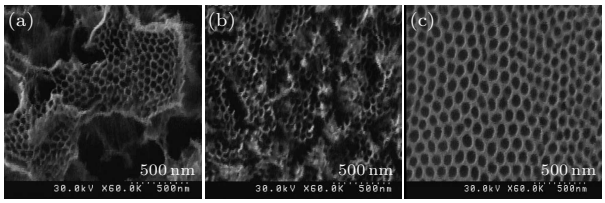

Fig. 3. SEM images of the nanotubes anodized in electrolyte solution containing (2 v%) deionized water and (0.3 wt.%) NH_4F and annealed at 450℃ for 1 h for different applied volts of (a) 35 V, (b) 45 V and (c) 55 V.

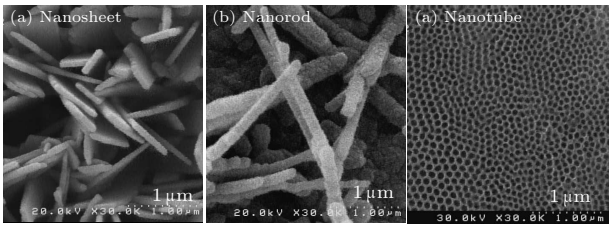

Fig. 4. SEM images of the TiO_2 nanostructures of (a) nanosheet synthesized in CVD at 850℃ for 1.5 h with Au catalyzer under Ar and C_3 H_6O (acetone) flow, (b) nanorod synthesized in CVD at 850℃ for 1.5 h with HCl treatment under Ar and C_3 H_6O (acetone) flow, and (c) nanotubes anodized at 55 V in electrolyte solution containing (2 v%) deionized water and (0.3 wt.%) NH_4F and annealed at 450℃ for 1 h.

TiO_2 nanorod, TiO_2 nanosheet and TiO_2 nanotubes were obtained in each part. The main purpose here was to study the effect of the morphological properties of TiO_2 nanostructures on the physical properties. The morphological observations such as length, width, diameter and wall thicknesses of the TiO_2 nanostructures are evaluated using field emission scanning electron microscopy (FESEM). Structural properties of the samples are studied by an x-ray diffractometer (XRD) using Cu $K\alpha$ radiation ($\lambda = 1.5418$ Å). Moreover, diffusion reflection spectra (DRS) are also obtained in the wavelength range 300–950 nm to calculate band gap energy of the samples using the optical absorption spectra.

The FE-SEM images of the TiO_2 nanorod,

nanosheet and nanotubes are shown in Fig. 4. As seen in Figs. 4(a) and 4(b), oxidation of terminated Ti foil using acetone as the oxygen source provides an excellent and simple method to fabricate well-aligned TiO_2 nanostructure arrays on a Ti substrate. The TiO_2 nanosheet in Fig. 4(a) was grown in different orientations without any perfect growth orientation but each sheet growing is controlled by the other neighboring sheets. The average thickness and width of the nanosheet are about 60 nm and 700 nm, respectively. These nanosheets are not parallel to each other but perpendicular to the substrate. In Fig. 4(b), TiO_2 nanorod arrays of large scale are formed on the Ti substrate. The nanorod length is 4 μm. The Ti oxidation process is described by several different models. Badescu and Momirlan[16] proposed that oxygen diffusion through the grain boundaries of the oxide layer and oxidation site is predominant at a temperature in the range of 800–1000℃. On the other hand, Czerwinski and Szpunar[14] showed that the TiO_2 grown at 900℃ is controlled by the surface diffusion of Ti on the sidewalls of pyramidal grains. In our case, the nanosheet and nanorod grown using acetone source had different morphologies from the samples grown in pure oxygen. When acetone is used for oxidation, the amount of oxygen for Ti oxidation process is much lower than the other growing condition like mixture of Ar with a low concentration of oxygen. Thus using acetone during the Ti oxidation caused diffusion of Ti species to the oxide surface as the predominant process and forming different nanostructures. As was seen, if the oxygen abundance is much higher than acetone, like pure oxygen, diffusion of oxygen will be more than Ti diffusion and cause formation of thin polycrystalline.[17]

Finally, the SEM image of Fig. 4(c) shows the top open and highly oriented TiO_2 nanotube. The diameters and wall thicknesses of tubes measured from SEM images are about 65 nm and 8 nm, respectively. Moreover, the growing of TiO_2 nanotubes can be explained through these processes:[18] (i) By applied anodization voltage on Ti alloy, stable compact oxide layer of Ti, TiO_2, is formed on the surface of the metal by electric field that is assisted between electrodes according to

$$\mathrm{Ti} + 2\mathrm{H_2O_2} \rightarrow \mathrm{TiO_2} + 2\mathrm{H^+} + 2\mathrm{e^-}.$$

(ii) The percentage of fluoride ions in electrolyte is responsible for the chemical dissolution and pores are formed on oxide–electrolyte interface to produce soluble $\mathrm{Ti(F_6)^{2-}}$ complex,

$$\mathrm{TiO_2} + 4\mathrm{H^+} + 6\mathrm{F^-} \rightarrow \mathrm{Ti(F_6)^{2-}} + 2\mathrm{H_2O_2}.$$

(iii) When these processes, chemical dissolution and oxidation, achieve a stable condition then TiO_2 nanotubes will be formed.

The crystal structure and phase of different nanostructures of TiO_2 nanorod, nanosheet and nanotubes are determined by XRD. The crystal phases of these structures are important for studying their different properties such as photoelectrochemistry and photocatalysis of the TiO_2.[19–21] The nanosheet and nanorod were heated in a mixture of Ar and acetone flow at 850℃ and the nanotubes were annealed at 450℃ in ambient air before XRD measurement.

It can be seen that all the samples are polycrystalline. For the nanosheet and nanorod samples, the diffraction peaks (110), (101), (111), (211), (002) and (112) are attributed to the tetragonal TiO_2 rutile phase that the lattice parameters of rutile TiO_2 are $a = b = 0.458$ nm and $c = 0.295$ nm (JCPDS file No. 20494). These XRD results show that nanorod and nanosheet samples have the same phase, rutile, and the intensities of these diffraction peaks for nanorod are significantly larger than the nanosheet intensity peaks. On the other hand, for the TiO_2 nanotubes anodized in (2 v%) DI water and (0.3 wt.%) NH_4F solution, the anatase phase is a dominant phase and the peaks corresponding to (101), (004), (105) and (220) planes appear only in the tubes sample patterns (JCPDS file No. 20387). Moreover, Ti peaks can also be seen only in the XRD spectra of tubes sample, which come from the Ti substrate used as the anode electrode in anodization and the two other samples do not show any Ti peaks. These phases changing for TiO_2 nanostructures may be caused by different annealing temperatures. It is expected that the growth process of TiO_2 nanostructures depends on the temperature and would affect the structure of the TiO_2 film. This is in good agreement with other researchers' motions that the TiO_2 anatase phase would appear at low temperatures, and rutile would appear at higher temperatures.[22,23]

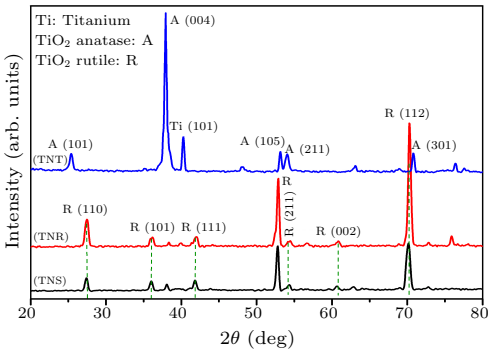

Fig. 5. XRD pattern of the TiO_2 nanostructures: (TNS) nanosheet, (TNR) nanorod and (TNT) nanotube.

One of the most useful optical observations is DRS to obtain electronic transitions of the material. The typical variation of diffuse reflectance of TiO_2 nanostructures is recorded in the wavelength range 300–950 nm, as shown in Fig. 6. As can be seen, sensitization of different TiO_2 nanostructures such as nanosheet, nanorod and nanotube shows different absorption edges since nanosheet spectra have the most shifting to red region. Different absorption edges can be related to their different crystal phases. Moreover, it shows that the intensity of nanotube reflection spectra is much greater than the other structures. The highest intensity of nanotube spectra may be caused by its highly ordered tube morphology.

As is seen in SEM images of Fig. 4, nanosheets and nanorods are grown in random directions without any preferred orientations but nanotube arrays are grown compacted and highly ordered. A highly ordered one-dimensional channel structure can provide a direct path for electrons, can promote the electron transport velocity, and can also cause reduction of the charge recombination.[22]

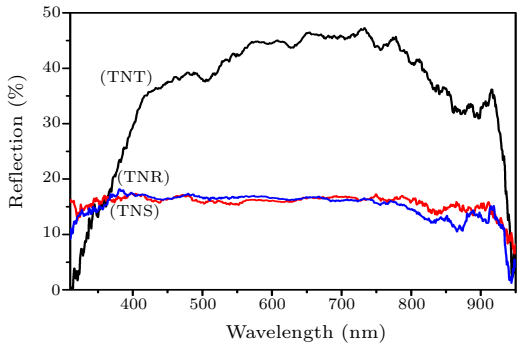

Fig. 6. DRS of the TiO_2 nanostructures: (TNS) nanosheet, (TNR) nanorod and (TNT) nanotube.

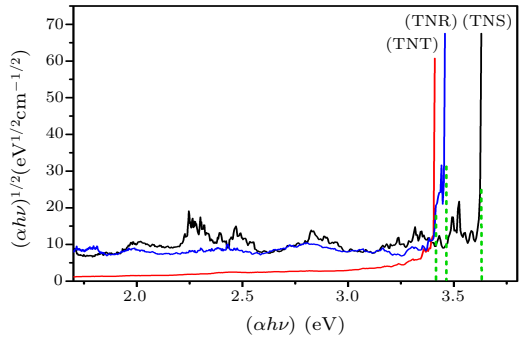

Fig. 7. Band gap energy of the TiO_2 nanostructures: (TNS) nanosheet, (TNR) nanorod and (TNT) nanotube.

Band gap energy was obtained using DRS from the Wood–Tauc equation as[23]

$$\alpha h\vartheta = \beta(h\vartheta - E_{\rm g})^m, \tag{1}$$

where h is a plank constant, ϑ is a frequency, α is an absorption coefficient, β is a proportionality constant, and m is a parameter for semiconductor direct transition and this value can be considered as 2. The band gap energies of TiO_2 nanostructures are estimated by plotting the tauc plot $\sqrt{\alpha h\vartheta}$ versus $h\vartheta$ with extra plotting line to the x-axis in Fig. 7.

The band gap energies of the nanosheet, nanorod and nanotube samples are determined to be about 3.6, 3.45, 3.4 eV, respectively. The differences among the band gap energies of these different structures of TiO_2 can be related to their crystal phases that can be obtained from the XRD patterns.

In summary, TiO_2 nanostructures with different morphologies have been synthesized by changing the experimental conditions such as growth methods, using different gases and process temperatures. It is observed that three different nanostructures of sheet, rod and tube are achievable. In comparison of the physical properties of these three nanostructures such as structural, morphological and optical, it is found that morphology, crystal structures and optical response can change correspondingly, which lead to the use of these nanostructures in different applications.

References

[1] Chen X and Mao S S 2007 *Chem. Rev.* **107** 2891
[2] Mor G K, Varghese O K, Paulose M, Shankar K and Grimes C A 2006 *Sol. Energy Mater. Sol. Cells* **90** 2011
[3] Kamat P V 2012 *J. Phys. Chem.* C **116** 11849
[4] Chen D and Caruso R A 2012 *Adv. Funct. Mater.* **22** 1966
[5] Daghrir R, Drogui P and Robert D 2013 *Ind. Eng. Chem. Res.* **52** 3581
[6] Movafaghi S et al 2016 *Lap Chip* **16** 3204
[7] Movafaghi S et al 2017 *Adv. Healthcare Mater.* **6** 1600717
[8] Tétreault N and Gratzel M 2012 *Energy Environ. Sci.* **5** 8506
[9] Zhang Q F and Cao G Z 2011 *J. Mater. Chem.* **21** 6769
[10] Mora-Ser I, Gimnez S, Fabregat-Santiago F, Gmez R, Shen Q, Toyoda T and Bisquert J 2009 *Acc. Chem. Res.* **42** 1848
[11] Grätzel M 2009 *Acc. Chem. Res.* **42** 1788
[12] Boschloo G, Hagfeldt A, Sun L, Kloo L and Pettersson H 2010 *Chem. Rev.* **110** 6595
[13] Rühle S, Shalom M and Zaban A 2010 *ChemPhysChem* **11** 2290
[14] Lan X, Bai J, Masala S, M Thon S, Ren Y et al 2013 *Adv. Mater.* **25** 1769
[15] Hoseinzadeh T, Ghorannevis Z and Ghoranneviss M 2017 *Appl. Phys.* A **123** 436
[16] Badescu V and Mormirlan M 1996 *J. Cryst. Growth* **169** 309
[17] Li S, Zhang G, Guo D, Ligang Yu and Zhang W 2009 *J. Phys. Chem.* C **113** 12759
[18] Czerwinski F and Szpunar J A 1998 *Micron* **29** 201
[19] Fujishima A, Rao T N and Tryk D A 2000 *J. Photochem. Photobiol.* C **1** 1
[20] Tryk D A, Fujishima A and Honda K 2000 *Electrochim. Acta* **45** 2363
[21] Herrmann J M 2005 *Top. Catalysis* **34** 49
[22] Yu J G and Wang B 2010 *Appl. Catal.* B **94** 295
[23] Wood D and Tauc J 1972 *Phys. Rev.* B **5** 3144